

Frontier molecular orbital analysis of $\text{Cu}_n\text{-O}_2$ reactivity

Peng Chen, Edward I. Solomon*

Department of Chemistry, Stanford University, Stanford, CA 94305, USA

Received 20 April 2001; received in revised form 18 June 2001; accepted 20 June 2001

Abstract

Frontier molecular orbital (FMO) theory coupled with density functional calculations has been applied to investigate the chemical reactivity of three key bioinorganic $\text{Cu}_n\text{-O}_2$ complexes, the mononuclear end-on hydroperoxo-Cu(II), the side-on bridged $\mu\text{-}\eta^2\text{:}\eta^2\text{-O}_2^{2-}$ Cu(II)₂ dimer and the bis- $\mu\text{-oxo}$ Cu(III)₂ dimer. Two acceptor orbitals (σ^* and π^*) of each complex and two types of donating substrates (σ -substrate, phosphine; π -substrate, alkylbenzene) are considered in the electrophilic attack mechanism. The angular dependences of different reaction pathways are determined using FMO theory and the angular overlap model. Including steric effects, the σ^*/σ and π^*/π pathways are found more reactive than the corresponding cross σ^*/π and π^*/σ pathways which have poor donor–acceptor orbital overlaps in the sterically constrained substrate access region. © 2002 Elsevier Science Inc. All rights reserved.

Keywords: Frontier molecular orbital; $\text{Cu}_n\text{-O}_2$ reactivity; Density functional calculations

1. Introduction

$\text{Cu}_n\text{-O}_2$ reactivity is one of the dominant areas in biological oxygen chemistry [1]. Oxygen reduction and activation by copper sites are ubiquitous in both homogeneous [2] and heterogeneous catalysis [3]. Dioxygen reduction to peroxide coupled to oxidation of substrate and activation for hydroxylation are observed in copper proteins which have mononuclear (amine oxidase and galactose oxidase) [4], non-coupled binuclear (dopamine β -monooxygenase and peptidylglycine α -hydroxylating monooxygenase) [4], coupled binuclear (tyrosinase and catechol oxidase) [5], and perhaps multinuclear (particulate-methane monooxygenase [6]) copper active sites. Three key complexes have been identified/proposed as intermediates in the catalytic mechanisms. A mononuclear end-on hydroperoxo-Cu(II) (referred to as hydroperoxo) complex is believed to be the catalytic intermediate in H-atom abstraction from substrate in the non-coupled binuclear copper enzymes [4]. A side-on bridged binuclear $\mu\text{-}\eta^2\text{:}\eta^2\text{-O}_2^{2-}$ Cu(II)₂ (referred to as side-on) complex is present in the coupled binuclear copper enzyme tyrosinase which catalyzes the electrophilic hydroxylation of phenol

[7]. In copper bioinorganic model chemistry, the side-on complex can be in rapid equilibrium with the bis- $\mu\text{-oxo}$ Cu(III)₂ isomer (referred to as bis- $\mu\text{-oxo}$) which has dominant H-atom abstraction chemistry [8]. All three complexes have been studied extensively in model chemistry, where electrophilic attack of π -electron density of aromatic rings (π -substrates) [9], oxo-transfer to PPh₃ [10] and H-atom abstraction from aliphatic C–H bonds [11,12] (σ -substrates) have been observed. Three representative model complexes with the aforementioned $\text{Cu}_n\text{-O}_2$ core structures (hydroperoxo [13], side-on [14], bis- $\mu\text{-oxo}$ [15]) are shown in Scheme 1.

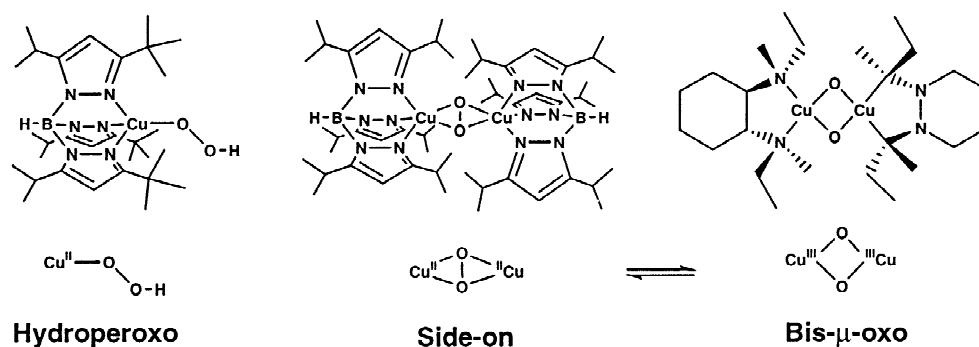
In frontier molecular orbital (FMO) theory [16–18], the energies, atomic orbital coefficients, net atomic charges and orbital overlaps of FMOs can be used to estimate relative chemical reactivity. The perturbation theory derived expression for the energy change (ΔE) upon overlap of two FMOs from two reactants is

$$\Delta E = -\sum_{ab} (q_a + q_b) \beta_{ab} S_{ab} + \frac{Q_k Q_l}{\epsilon R_{kl}} + \frac{2(\sum_{ab} c_{ra} c_{sb} \beta_{ab})^2}{E_r^{\text{occ.}} - E_s^{\text{unocc.}}} \quad (1)$$

where q_a and q_b are the electron populations in the atomic orbitals a and b, β and S are the resonance and overlap integrals, Q_k and Q_l are the total charges on atom k and l, ϵ is the local dielectric constant, R_{kl} is the distance between the atom k and l, c_{ra} is the coefficient of atomic

*Corresponding author. Tel.: +1-650-8513-607; fax: +1-650-7250-2599.

E-mail address: edward.solomon@stanford.edu (E.I. Solomon).



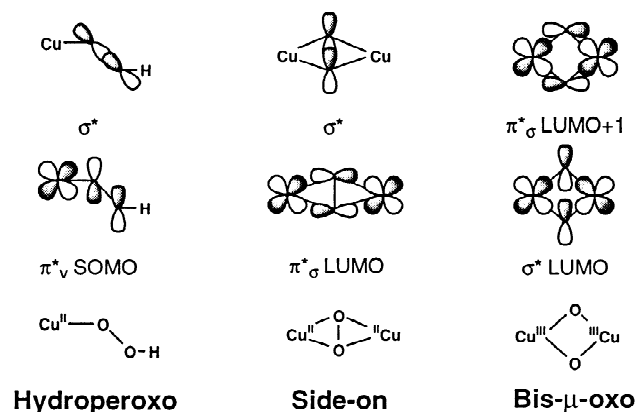
Scheme 1.

orbital a in molecular orbital r (r refers to the molecular orbital on one molecule and s refers to that on the other), E_r is the energy of molecular orbital r (occ., occupied; unocc., unoccupied). The first term is the first order close-shell repulsion term and is similar for different reaction pathways of similar reactants. This is normally neglected in the consideration of differential reactivity. The second term is the charge term-Coulombic repulsion or attraction. The third term is the FMO term, which represents the interaction of the occupied orbital on the electron donor with the unoccupied/partially occupied orbital on the electron acceptor, where the energy separation of interacting FMOs, atomic orbital coefficients and orbital overlap ($\beta^2 \propto S^2$, which is angle dependent) play important roles.

The electronic structures and thus the FMOs of the three $\text{Cu}_n\text{-O}_2$ complexes in Scheme 1 have been extensively studied [13,19,20]. The singly occupied molecular orbital (SOMO) of the hydroperoxo complex is the antibonding $\text{Cu } d_{x^2-y^2}$ orbital with significant contribution from the out of plane (the Cu-O-O plane) peroxide π^* orbital (designated π^*_v) [13]. The side-on complex LUMO is the antibonding combination of the in-plane (the Cu_2O_2 plane) peroxide π^* orbital (designated π^*_σ) with the two Cu(II) $d_{x^2-y^2}$ orbitals [19]. In these two complexes, the peroxide σ^* orbitals are higher in energy but activated by the protonation in the hydroperoxo complex or the strong σ -donation to the coppers in the side-on complex. The bis- μ -oxo complex is isoelectronic with the side-on complex. However, the cleaved O-O bond strongly stabilizes the peroxide σ^* orbital which now makes a large contribution to the LUMO of the bis- μ -oxo complex, while the antibonding component of the peroxide π^*_σ orbital is in the LUMO + 1 [20]. These are illustrated in Scheme 2. The HOMOs of the σ -substrate PPh_3 and π -substrate alkylbenzene are well understood [21,22]. The phosphine HOMO is the lone pair σ -donor orbital on the phosphorus while the alkylbenzene HOMO is a π -type molecular orbital perpendicular to the plane of the ring. The substrate orbital in the H-atom abstraction reaction is an aliphatic C-H bond, which is a σ -type orbital similar to the phosphine HOMO.

Recently, FMO theory has been coupled with spectrosc-

copically calibrated density function theory (DFT) calculations, which give detailed information about the FMOs of the reactants, to obtain insight into biological $\text{Cu}_n\text{-O}_2$ chemistry [13,20,23,24]. Aromatic hydroxylation through electrophilic attack by the side-on complex at the benzene HOMO π -electron density has been shown to involve the π -overlap of the side-on LUMO, which contains a significant contribution of the peroxide π^*_σ orbital, with the p_π orbital of the carbon atom on the ring [23]. The studies have been further extended to the bis- μ -oxo [20] and hydroperoxo complexes [13]. Two dominant reaction pathways have been identified [24]. The π^*/π pathway involves the peroxide π^* orbital component in the LUMOs of $\text{Cu}_n\text{-O}_2$ complexes (LUMO+1 in the bis- μ -oxo) and π -electrons of aromatic substrates. The side-on complex is found most reactive toward aromatic hydroxylation. The σ^*/σ pathway involves the peroxide σ^* orbital, which is activated in the $\text{Cu}_n\text{-O}_2$ complexes, and the σ -donor orbitals of substrates (e.g. PPh_3 and aliphatic C-H bond). In this case, the bis- μ -oxo complex is found most efficient in oxo-transfer and H-atom abstraction, dependent on steric effects in the former. In this study we determine the angular dependence of these different reaction pathways, evaluate the possibilities of cross reaction pathways (π^*/σ and σ^*/π) and show how steric effects limit these cross pathways.



Scheme 2.

2. Calculation details

Density functional calculations were performed on a SGI Origin 2000 workstation, using Gaussian 98 [25]. Becke's three-parameter hybrid functional with the correlation functional of Lee, Yang and Parr (B3LYP) [26] was used for all DFT calculations. A general basis set (6-311G* for Cu and 6-31G* for all other atoms) was used. Convergence was reached when the relative change in the density matrix between subsequent iterations was less than 1×10^{-4} . Wavefunctions were plotted with the visualization program Molden [27]. Calculated molecular orbital energies were referenced to the carbon 1s electron binding energy.

The hydroperoxo model was taken from a previous study [13]. The crystal structures of the $[\text{Cu}(\text{HB}(3,5\text{-}i\text{-Pr}_2\text{Pz})_3)_2(\text{O}_2)]$ [14] and $[(L_{\text{ME}})_2\text{Cu}_2(\mu_2\text{-O})_2]^{2+}$ [15] complexes were used for the side-on and bis- μ -oxo models. Side chains were truncated to simplify the calculations. Geometry optimized PEt_3 and ethylbenzene are used to model PPh_3 and alkylbenzene, respectively.

The angular overlap model (AOM) was used to calculate the angular dependence of orbital overlaps (S and S^2) [28]. Standard AOM transformation matrices were used [29]. Resonance integrals were calculated using Wolfsberg–Helmholz approximation $\beta_{ab} \approx k[(H_{aa} + H_{bb})/2]S_{ab}$ where $k \approx 2$. Atomic overlap integrals were taken from DFT calculations

using oxygen 2p, carbon 2p, and phosphorus 3p orbitals in STO-3G basis set at $R_{\text{OP}} = 1.4 \text{ \AA}$, $R_{\text{OC}} = 1.2 \text{ \AA}$ where the σ radial overlaps are at the maximum (Fig. S1). Molecular orbital energies, coefficients and atomic charges were taken from DFT calculations. Steric effects were obtained using the space-filling model in the program RasMol [30] where complete molecular structures were used (Scheme 1).

3. Results and analysis

3.1. DFT calculated FMOs

Fig. 1 shows the 3-D contours of the FMOs for the three $\text{Cu}_n\text{-O}_2$ complexes (hydroperoxo, side-on and bis- μ -oxo), a σ -type substrate phosphine and a π -type substrate alkylbenzene from spin-unrestricted DFT calculations. Two unoccupied/singly occupied Cu-peroxide antibonding FMOs with significant peroxide contributions are shown for each $\text{Cu}_n\text{-O}_2$ complex, labeled σ^* and π^*_σ (π^*_ν for hydroperoxo) according to the nature of the peroxide orbital component. The σ^* orbitals are σ -acceptors in the FMO considerations with the σ^* orbital of the bis- μ -oxo much lower in energy than the other two complexes due to the cleavage of O–O bond. The π^*_σ/π^*_ν orbitals can be π

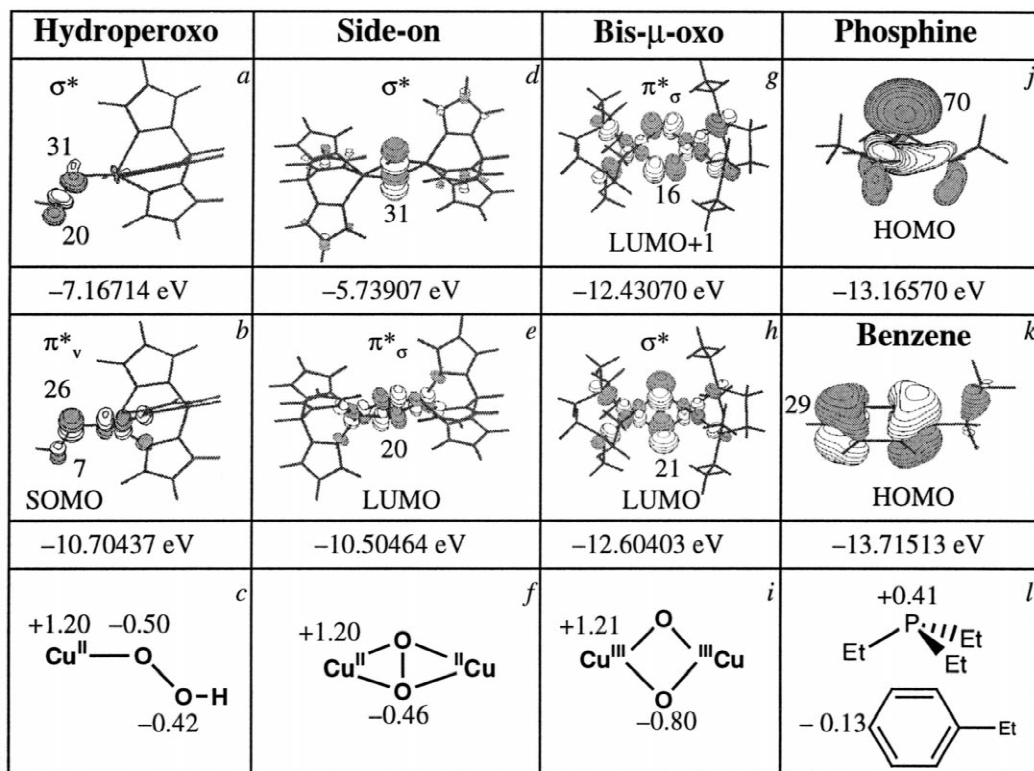


Fig. 1. 3-D contours of the relevant DFT calculated FMOs for the hydroperoxo, side-on, bis- μ -oxo $\text{Cu}_n\text{-O}_2$ complexes, and the phosphine and alkylbenzene substrates (upper and middle rows). Orbital coefficients are labeled next to the contours. MO energies are labeled below. The relevant atomic charges are labeled on the core structures (bottom row).

or σ -acceptors depending on the orientation of substrate attack. The π^*_v orbital of the hydroperoxo has a very small coefficient on the distal oxygen atom due to the bond polarization by protonation.

The HOMO of the phosphine substrate is the lone pair orbital (Fig. 1j), which is a σ -donor. The substrate alkylbenzene HOMO is a π -type orbital, which can be a π -donor or a pseudo σ -donor if attacked from the side (Fig. 1k). Relevant molecular orbital coefficients, MO energies and atomic charges are given. The calculated electronic structures are consistent with previous spectroscopic and theoretical studies [13,19,20], which justifies their use in the FMO analysis of the angular dependence of the reactivities in the different reaction pathways.

3.2. Angular dependence of the FMO term

Scheme 3A defines the polar angles θ and ϕ of attack when the substrates approach the peroxide moiety of the $\text{Cu}_n\text{-O}_2$ complexes in a general coordinate system, where θ is the angle between the attack direction and the z -axis, and ϕ is the angle between the projected attack direction onto the xy plane and the x -axis. For the hydroperoxo complex, the z -axis is placed along the O–O bond and the x -axis is perpendicular to the Cu–O–O plane pointing out of the paper (Scheme 3B). A common coordinate system is used for both the side-on and bis- μ -oxo complexes. The z -axis is placed along the O–O bond, the x -axis is along the Cu–Cu direction and y -axis is perpendicular to the Cu_2O_2 plane (Scheme 3C). Two substrates are considered here, the σ -substrate phosphine and the π -substrate alkylbenzene. Scheme 3 illustrates the substrate orientations for attack of the $\text{Cu}_n\text{-O}_2$ complexes. The alkylbenzene has an additional torsion angle ψ (Scheme 3C), which is set at 0° when the benzene ring is in the yz plane. For all angles, the smallest repeat is 0 to 90° which is the range considered here.

3.2.1. σ -substrates (phosphine)

Fig. 2 shows the θ dependence of the FMO term for the chemical reactivity (ΔE) of the hydroperoxo, side-on and

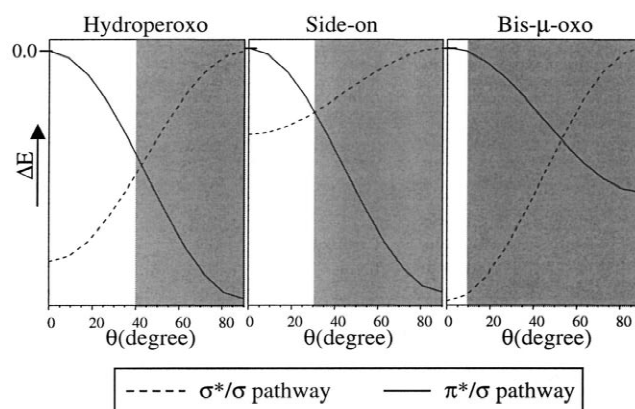
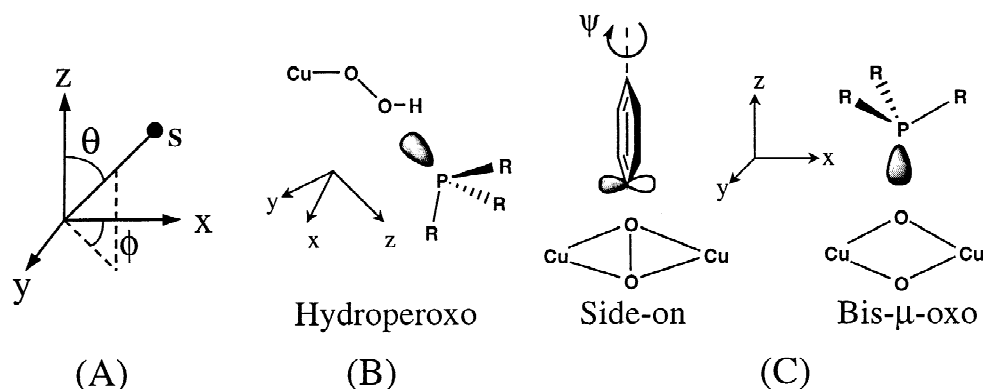


Fig. 2. θ angular dependence of the chemical reactivity FMO term (ΔE) of the hydroperoxo (left), side-on (middle) and bis- μ -oxo (right) complexes with the σ -substrate phosphine. Dashed line, the σ^*/σ pathway; solid line, the π^*/σ pathway. Shaded areas in the plots indicate inaccessible regions limited by steric effects.

bis- μ -oxo complex with the σ -substrate phosphine at $\phi=0$ in Scheme 3. The relative reactivities of the different complexes are not considered due to the additional contribution of the first term in the FMO analysis (Eq. (1)). Sinusoidal dependence is found for both σ^*/σ and π^*/σ pathways, where the former pathway involves the σ^* orbitals of the $\text{Cu}_n\text{-O}_2$ complexes as the electron acceptors and the latter, the π^* (π^*_σ/π^*_v) orbitals of the $\text{Cu}_n\text{-O}_2$ complexes as the acceptor (Fig. 1). (The relative difference of the σ^*/σ and π^*/σ pathways in each complex results from the different orbital coefficients and MO energies.) The donor is the σ -HOMO of the phosphine (Fig. 1j). The σ^*/σ pathways for all three complexes are more reactive (more negative $\Delta E \Rightarrow$ more reactive) in the small θ value region of the plots in Fig. 2 than the π^*/σ pathways and the ΔE 's go from most negative at $\theta=0^\circ$ to zero at $\theta=90^\circ$. The π^*/σ pathways have the opposite angular dependence and are more reactive in the large θ value region. The FMO term angular dependence of the σ^*/σ pathways comes from the obvious angular dependence of the orbital overlap between the acceptor orbital σ^* of the three complexes and the σ donor phosphine HOMO. In contrast,



Scheme 3.

for the π^*/σ pathways, the p_π atomic components of the acceptor π^* orbitals on the oxygen atoms are oriented perpendicular to the σ^* orbitals (Fig. 1), which leads to the opposite trend in the angular dependence of the donor–acceptor overlap with increasing θ .

Varying the ϕ angle does not change the donor–acceptor overlap for the σ^*/σ pathways due to the σ -symmetry (Fig. 1). However, increasing the ϕ angle will further decrease the donor–acceptor overlap for the π^*/σ pathways since the oxygen p_π components of the π^* orbitals lie along the x -axis and the donor–acceptor overlap will be zero when $\phi=90^\circ$ even if θ is 90° .

It is important to note that not all values of the θ angle are allowed when the reactants are brought together due to steric effects. Space-filling molecular modeling shows that the allowed θ angle is no larger than 40° when PPh_3 approaches the hydroperoxo complex due to the steric limits of the bulky side chains on the trispyrazolylborate ligand and the three phenyl groups of PPh_3 . The analogous θ cutoff values for the side-on and bis- μ -oxo complexes are 30° and 10° , respectively. The shaded areas in Fig. 2 show the sterically inaccessible regions for the three $\text{Cu}_n\text{-O}_2$ complexes. Thus, when the steric effects are included, the σ^*/σ pathway is more reactive than the cross π^*/σ pathway for all three $\text{Cu}_n\text{-O}_2$ complexes.

3.2.2. π -substrates (alkylbenzene)

Fig. 3 gives the θ dependence of the FMO term of chemical reactivity for all three complexes with the π -substrate alkylbenzene at $\phi, \psi=0$. Sinusoidal dependence is also observed for both σ^*/π and π^*/π pathways, where the donor orbital is the π -type alkylbenzene HOMO (Fig. 1k). The π^*/π pathways for all three complexes are more reactive in the small θ value region than the σ^*/π pathways and the ΔE 's go from most negative at $\theta=0^\circ$ to zero at $\theta=90^\circ$. Again, the crossed σ^*/π pathways have the opposite trend and are more reactive in the larger θ

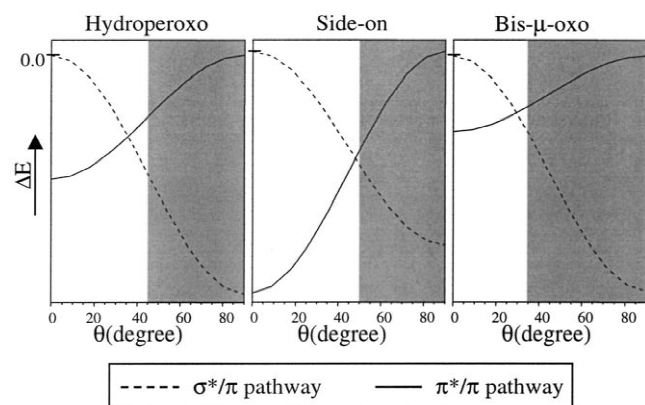


Fig. 3. θ angular dependence of the chemical reactivity FMO term (ΔE) of the hydroperoxo (left), side-on (middle) and bis- μ -oxo (right) complexes with the π -substrate alkylbenzene. Dashed line, the σ^*/π pathway; solid line, the π^*/π pathway. Shaded areas in the plots indicate inaccessible regions limited by steric effects.

value region. These angular dependences come from the donor–acceptor orbital overlaps, similar to those discussed above. Increasing the ϕ angle decreases the donor–acceptor overlap for the π^*/π pathways without affecting the σ^*/π pathways, while increasing the ψ angle lowers the donor–acceptor overlap for both pathways.

Space-filling molecular modeling gives cutoff values for the θ angle due to the steric effects of the $\text{Cu}_n\text{-O}_2$ complexes and the alkylbenzene substrate. The shaded areas in Fig. 3 show the sterically inaccessible regions. Thus, including steric effects, the π^*/π pathway is more reactive than the cross σ^*/π pathway for all three complexes.

4. Discussion

This study has determined the angular dependence of the chemical reactivities of different reaction pathways involved in three $\text{Cu}_n\text{-O}_2$ complexes, the hydroperoxo, side-on and bis- μ -oxo models. Two substrates are considered: the σ -substrate phosphine and the π -substrate alkylbenzene. The cross π^*/σ and σ^*/π pathways are found less reactive than the σ^*/σ and π^*/π pathways which have better donor–acceptor orbital overlaps in the sterically allowed angle region of substrate attack.

For the hydroperoxo complex, the π^*/σ pathway requires that the phosphine substrate approaches the distal oxygen atom below the O–O–H plane in order for its σ HOMO to have reasonable overlap with the hydroperoxo π^*_v orbital (Fig. 1b). The accessibility is limited by the *tert*-butyl side chains on the trispyrazolylborate ligand (Scheme 1, left). The sterically allowed θ angle region is $0\text{--}40^\circ$ where the overlap is poor and the σ^*/σ pathway dominates (Fig. 2, left). Similarly, the σ^*/π pathway requires tilting the aromatic ring of alkylbenzene substrate upon attack in order for its π -type HOMO to have good overlap with the hydroperoxo σ^* orbital. The accessible θ angle region is only $0\text{--}45^\circ$ where the reactivity is low and the corresponding π^*/π pathway dominates (Fig. 3, left).

The side-on and bis- μ -oxo complexes have similar core structures and FMOs, except that the bis- μ -oxo core is more compact than the side-on core [14,15]. For the σ -substrate phosphine, the σ^*/σ pathway is more reactive than the cross π^*/σ pathway in both complexes due to the good donor–acceptor orbital overlaps at the least steric substrate orientation ($\theta=0^\circ$). Fig. 4A schematically shows this overlap for the bis- μ -oxo σ^* with the phosphine HOMO where the DFT calculated FMOs are used for illustration. In contrast, in order for the π^*/σ pathway to have a good donor–acceptor orbital overlap between the side-on/bis- μ -oxo π^*_σ and the phosphine HOMO, the phosphine substrate has to approach from the side, where the Cu ligands interfere with phenyl rings of PPh_3 . This steric hindrance is schematically shown in Fig. 4B for the bis- μ -oxo complex. The angle θ can only be $<10^\circ$ based

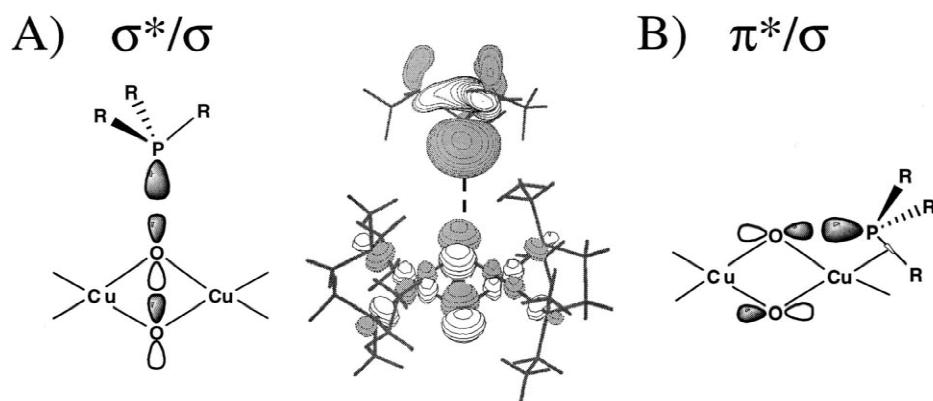


Fig. 4. (A) Good donor–acceptor overlap for the σ^*/σ pathway. (B) The sterically hindered π^*/σ pathway.

on molecular modeling. The less compact side-on complex core allows more freedom in θ attack angle (Fig. 2, middle).

Due to the compactness of the bis- μ -oxo core, the radial accessibility for the bulky PPh_3 substrate to the peroxide moiety is an additional factor that will limit the donor–acceptor orbital overlap (Fig. S1). This steric factor is likely the reason for the observed ineffectiveness of oxo-transfer to PPh_3 of one bis- μ -oxo complex [31], where limited radial accessibility results in significant separation between the substrate and the reactant, which decreases the

donor–acceptor orbital overlap and eliminates the reactivity. In contrast, a similar bis- μ -oxo complex with less bulky ligands converts PPh_3 to OPPh_3 nearly quantitatively. In the case of the dimeric side-on $[\text{Cu}(\text{HB}(3,5\text{-}i\text{Pr}_2\text{Pz})_3)](\text{O}_2)$ complex [32], steric hindrance of the alkyltrispyrazolyl ligand directs the bulky PPh_3 substrate to attack the metal center rather than the peroxide and the deoxygenation–substitution reaction product is generated.

For the π -substrate alkylbenzene, the π^*/π pathway is more reactive than the cross σ^*/π pathway in both Cu_2O_2 complexes. The orientation of benzene ring, which has the

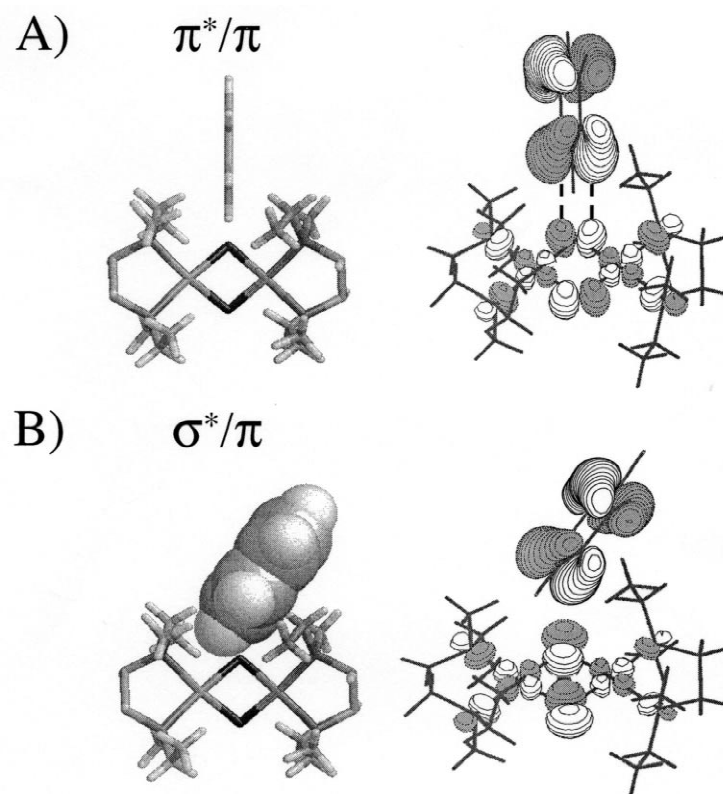


Fig. 5. (A) The orientation of least steric repulsion for the π -substrate alkylbenzene attack on the bis- μ -oxo complex (left), and the corresponding good donor/acceptor orbital overlap of the π^*/π pathway (right). (B) Space-filling model of the alkylbenzene orientation at the largest possible ϕ value (35°) upon attack on the bis- μ -oxo complex (left), and the corresponding donor–acceptor orbital overlap of the σ^*/π pathway (right).

least steric repulsion with the Cu_2O_2 core, is shown in Fig. 5A, left, for the bis- μ -oxo complex. The good overlap between the donor benzene π HOMO and the acceptor π^*_σ orbital is shown in Fig. 5A, right. This donor–acceptor overlap results in the increased chemical reactivity of the π^*/π pathways in both the side-on and bis- μ -oxo complexes. In contrast, for the σ^*/π pathway to gain significant donor–acceptor overlap, the benzene ring has to tilt and the steric repulsion limits the angle θ to 35° for the bis- μ -oxo complex (50° for the side-on). This steric limitation is illustrated for the bis- μ -oxo complex using space-filling model in Fig. 5B, left. The resultant donor benzene π HOMO and acceptor bis- μ -oxo σ^* orbital overlap is shown in Fig. 5B, right, which is still poor and leads to low chemical reactivity (Fig. 3, right). Although the benzene ring can rotate from the $\phi=0^\circ$ to the $\phi=90^\circ$ orientation with $\theta=90^\circ$ (Fig. S2) which gives good overlap of its HOMO with the bis- μ -oxo(side-on) σ^* orbital, the side chains of the ligand of the bis- μ -oxo complex interact with the benzene ring, which keeps the substrate and the bis- μ -oxo complex apart ($>3.5 \text{ \AA}$) leading to poor radial overlap (Fig. S1).

In summary, we have determined the angular dependence of different reaction pathways of the $\text{Cu}_n\text{-O}_2$ complexes using FMO theory and the angular overlap model. Coupled with steric considerations, the cross σ^*/π and π^*/σ pathways are found less reactive than the corresponding σ^*/σ and π^*/π pathways, due to their poor donor–acceptor orbital overlaps in the sterically constrained substrate attack region.

Acknowledgements

This research is funded by the NIH (DK31450). P.C. is supported by the Gerhard Casper Stanford Graduate Fellowship. Supplementary Material. Interatomic distance dependence of atomic orbital overlap, Fig. S1, and additional molecular modeling, Fig. S2 are available.

References

- [1] R.H. Holm, P. Kennepohl, E.I. Solomon, *Chem. Rev.* 96 (1996) 2239.
- [2] N. Kitajima, Y. Moro-oka, *Chem. Rev.* 94 (1994) 737.
- [3] E.I. Solomon, P.M. Jones, J.A. May, *Chem. Rev.* 93 (1993) 2623.
- [4] J.P. Klinman, *Chem. Rev.* 96 (1996) 2541.
- [5] E.I. Solomon, U.M. Sundaram, T.E. Machonkin, *Chem. Rev.* 96 (1996) 2563.
- [6] H.H.T. Nguyen, A.K. Shiemke, S.J. Jacobs, B.J. Hales, M.E. Lidstrom, S.I. Chan, *J. Biol. Chem.* 269 (1994) 14995.
- [7] R.S. Himmelwright, N.C. Eickman, C.D. LuBien, K. Lerch, E.I. Solomon, *J. Am. Chem. Soc.* 102 (1980) 7339.
- [8] J.A. Halfen, S. Mahapatra, E.C. Wilkinson, S. Kaderli, V.C. Young Jr., L. Que Jr., A.D. Zuberhuhler, W.B. Tolman, *Science* 271 (1996) 1397.
- [9] K.D. Karlin, J.C. Hayes, Y. Gultneh, R.W. Cruse, J.W. McKown, J.P. Hutchinson, J. Zubieta, *J. Am. Chem. Soc.* 106 (1984) 2121.
- [10] N. Kitajima, K. Fujisawa, Y. Moro-oka, *Inorg. Chem.* 29 (1990) 357.
- [11] S. Mahapatra, J.A. Halfen, W.B. Tolman, *J. Am. Chem. Soc.* 118 (1996) 11575.
- [12] S. Itoh, M. Taki, H. Nakao, P.L. Holland, W.B. Tolman, L. Que Jr., S. Fukuzumi, *Angew. Chem. Int. Ed.* 39 (2000) 398.
- [13] P. Chen, K. Fujisawa, E.I. Solomon, *J. Am. Chem. Soc.* 122 (2000) 10177.
- [14] N. Kitajima, K. Fujisawa, Y. Moro-oka, *J. Am. Chem. Soc.* 111 (1989) 8975.
- [15] V. Mahadevan, Z. Hou, A. Cole, D.E. Root, T.K. Lal, E.I. Solomon, T.D.P. Stack, *J. Am. Chem. Soc.* 119 (1997) 11996.
- [16] G. Klopman, *J. Am. Chem. Soc.* 90 (1968) 223.
- [17] L. Salem, *J. Am. Chem. Soc.* 90 (1968) 543.
- [18] L. Salem, *J. Am. Chem. Soc.* 90 (1968) 553.
- [19] P.K. Ross, E.I. Solomon, *J. Am. Chem. Soc.* 112 (1990) 5871.
- [20] M.J. Henson, P. Mukherjee, D.E. Root, T.D.P. Stack, E.I. Solomon, *J. Am. Chem. Soc.* 121 (1999) 10332.
- [21] L. Salem, *The Molecular Orbital Theory of Conjugated Systems*, W.A. Benjamin, New York, 1966.
- [22] M. Karplus, R.N. Porter, *Atoms and Molecules an Introduction for Students of Physical Chemistry*, W.A. Benjamin, Philippines, 1970.
- [23] E. Pidcock, H.V. Obias, C.X. Zhang, K.D. Karlin, E.I. Solomon, *J. Am. Chem. Soc.* 120 (1998) 7841.
- [24] E.I. Solomon, P. Chen, M. Metz, S.-K. Lee, A.E. Palmer, *Oxygen binding, activation and reduction to water by copper proteins*, *Angew. Chem., Int. Ed. Engl.* (in press).
- [25] M.J. Frisch, G.W. Trucks, H.B. Schlegel, P.M.W. Gill, B.G. Johnson, M.A. Robb, J.R. Cheeseman, T.A. Keith, G.A. Peterson, J.A. Montgomery, K. Raghavachari, M.A. Al-Laham, V.G. Zakrzewski, J.V. Ortiz, J.B. Foresman, J. Cioslowski, B.B. Stefanov, A. Nanayakkara, M. Challacombe, C.Y. Peng, P.Y. Ayala, W. Chen, M.W. Wong, J.L. Andres, E.S. Replogle, R. Gomperts, R.L. Martin, D.J. Fox, J.S. Binkley, D.J. Defrees, J. Baker, J.P. Stewart, M. Head-Gordon, C. Gonzalez, J.A. Pople, *Gaussian 94/98*, Gaussian, Inc., Pittsburgh, 1995.
- [26] A.D. Becke, *J. Chem. Phys.* 98 (1993) 5648.
- [27] G. Schaftenaar, J.H. Noordik, *J. Comput.-Aided Mol. Des.* 14 (2000) 123.
- [28] A.B.P. Lever, *Inorganic Electronic Spectroscopy*, Elsevier, Amsterdam, 1984.
- [29] C.E. Schaffer, *Struct. Bonding* 5 (1968) 68.
- [30] R. Sayle, *RasMol*, Glaxo Research and Development, Greenford, Middlesex, UK, 1993.
- [31] V. Mahadevan, M.J. Henson, E.I. Solomon, T.D.P. Stack, *J. Am. Chem. Soc.* 122 (2000) 10249.
- [32] N. Kitajima, K. Fujisawa, C. Fujimoto, Y. Moro-oka, S. Hashimoto, T. Kitagawa, K. Toriumi, K. Tatsumi, A. Nakamura, *J. Am. Chem. Soc.* 114 (1992) 1277.